



Cite this: *CrystEngComm*, 2015, 17,
7938

Polyoxometalate-based metal–organic coordination networks for heterogeneous catalytic desulfurization†

Yuan-Yuan Ma,^a Hua-Qiao Tan,^{*a} Yong-Hui Wang,^a Xiu-Li Hao,^{*ab} Xiao-Jia Feng,^{ac} Hong-Ying Zang^a and Yang-Guang Li^{*a}

Three new polyoxometalate (POM)-based metal–organic coordination networks (MOCNs) with chemical formulae of $[Co(BBTZ)_{1.5}(HBBTZ)(H_2O)_2][PW_{12}O_{40}] \cdot H_2O$ (**1**), $[Co_{2.5}(BBTZ)_4(H_2O)_2][BW_{12}O_{40}] \cdot 4H_2O$ (**2**) and $[Cu(BBTZ)_2]_5[BW_{12}O_{40}]_2 \cdot 4H_2O$ (**3**) ($BBTZ = 1,4\text{-bis-(1,2,4-triazol-1-ylmethyl)benzene}$) were hydrothermally synthesized in a reaction system containing Keggin-type POMs, transition metal salts (cobalt salts and copper salts) and BBTZ ligands. All compounds were characterized by elemental analyses, IR, powder X-ray diffraction, TG analyses and single-crystal X-ray diffraction analyses. Compound **1** exhibits a POM-encapsulated 3-D supramolecular network, while compounds **2** and **3** display POM-supported 3-D coordination networks. Using the oxidative desulfurization of dibenzothiophene (DBT) as the model, the catalytic activities of compounds **1**–**3** are investigated. All three compounds show efficient catalytic activity for the oxidation of DBT with the order of **2** > **3** > **1**. It is found that the POM species of compounds **1**–**3** play the main role in the catalytic oxidative desulfurization process, while the TM ions, the loading amounts of POMs, and the structural features of these POM-based MOCNs are also necessary factors that affect the catalytic activities. Furthermore, a surfactant-assisted hydrothermal synthesis method has been developed to prepare nanocrystal **2**. SEM reveals that the as-synthesized nanocrystalline **2** is about 245 nm in diameter. The catalytic oxidative desulfurization experiments show that nanocrystal **2** possesses much higher catalytic activities than those of the large single-crystal products of **2**.

Received 1st August 2015,
Accepted 14th September 2015

DOI: 10.1039/c5ce01533b

www.rsc.org/crystengcomm

Introduction

The desulfurization of fossil fuels is a currently significant task, which is directly associated with the living environment of human beings.¹ In this research field, oxidative desulfurization has been considered as an effective strategy to remove refractory organosulfur substrates. To date, a key factor in this aspect is the exploration of new oxidative catalyst systems.² Polyoxometalates (POMs), as unique metal–oxo clusters of early transition metals (such as Mo, W, V, Nb and Ta), have been proved to be one of the most promising kinds of catalysts for desulfurization³ because of their excellent

controllability in composition, structure, charge and redox properties at the molecular level. However, POMs sometimes show good solubility in the reaction system, and act as homogeneous catalysts with a poor recovery.⁴ Furthermore, some POMs may suffer from hydrolyzation in different pH of solution, which must be surmounted in the homogeneous system.⁵ Moreover, the low specific surface area and the relatively low loading amount of POMs as heterogeneous catalysts also inhibit their catalytic applications.⁶ Therefore, developing a new type of POM-based catalytic materials with good stability, easy recycling, and high efficient catalytic activity is one of the currently challenging issues.

It is well known that metal–organic coordination networks (MOCNs) usually possess good stability and relatively low solubility in solutions.⁷ The introduction of POMs into MOCNs usually can not only load and disperse POM units into MOCNs at the molecular level, but also keep the redox activity of POM species well. Based on such consideration, a series of POM-based MOCNs have been constructed as heterogeneous catalysts.⁸ In these compounds, a few of them show good catalytic activities due to their porous structural features, which allow the contact between reactants and the catalytic active sites (POMs).⁹ In comparison with these

^a Key Laboratory of Polyoxometalate Science of Ministry of Education Faculty of Chemistry, Northeast Normal University, Changchun, 130024, PR China.

E-mail: tanhq870@nenu.edu.cn, liyg658@nenu.edu.cn

^b School of Chemical and Biological Engineering, Taiyuan University of Science and Technology, Taiyuan, 030021, PR China. E-mail: Haoxiuli1@163.com

^c College of Science, Shenyang Agricultural University, Shenyang, 110866, PR China

† Electronic supplementary information (ESI) available: Summary of selected bond lengths and angles; catalytic experiment data; IR, TG and PXRD and cif files of **1**–**3**. CCDC 1063971 (**1**), 1063960 (**2**) and 1401904 (**3**). For ESI and crystallographic data in CIF or other electronic format see DOI: 10.1039/c5ce01533b

limited porous compounds, numerous non-porous POM-based MOCNs have still been so far unexplored as heterogeneous catalysts.¹⁰ Thus, it is significant to develop new strategies to improve the catalytic activities of these non-porous hybrid compounds so as to explore new catalysts for oxidative desulfurization.

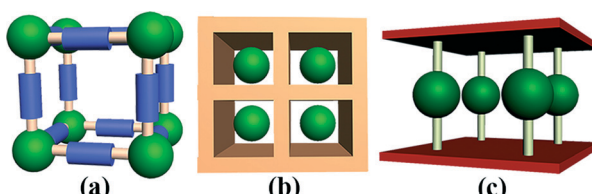
Generally, POMs can act as nodes, templates and pillars (Scheme 1) in POM-based MOCNs.^{11,12} In any case, a main concern is how to introduce more POM units into the MOCN skeletons and let them be exposed as much as possible in the reaction system. In this aspect, the combination of cationic MOCNs and various polyoxoanion units is an effective way to maximize the loading amount of POMs. Following this strategy, we have constructed many POM-based cationic MOCNs by the hydrothermal reaction of polyoxoanions, transition metal (TM) cations and various neutral *N*-donor bridging ligands.¹³ Although the loading amounts of POMs in our previous work^{9b,13d} have been significantly improved (about 71%), their catalytic activities for oxidation desulfurization are still relatively low. The factors that affect the catalytic activity of these catalysts remain unexplored.

Herein, we report three new POMs-based cationic MOCN compounds: $[\text{Co}(\text{BBTZ})_{1.5}(\text{HBBTZ})(\text{H}_2\text{O})_2][\text{PW}_{12}\text{O}_{40}] \cdot \text{H}_2\text{O}$ (1), $[\text{Co}_{2.5}(\text{BBTZ})_4(\text{H}_2\text{O})_2][\text{BW}_{12}\text{O}_{40}] \cdot 4\text{H}_2\text{O}$ (2) and $[\text{Cu}(\text{BBTZ})_{2.5}[\text{BW}_{12}\text{O}_{40}]_2 \cdot 4\text{H}_2\text{O}$ (3) (BBTZ = 1,4-bis-(1,2,4-triazol-1-ylmethyl) benzene). Using the oxidative desulfurization of dibenzothiophene (DBT) as the model, we confirm that all three compounds exhibit effective catalytic activity for the oxidation of DBT with the order of $2 > 3 > 1$. The effects of POMs, transition metal cations, the loading amount of POMs, and the structural features on the catalytic activities of compounds 1–3 have been investigated. Furthermore, a surfactant-assisted hydrothermal synthesis method is developed for the preparation of nanocrystalline compound 2 with a high specific surface area. SEM reveals that the as-synthesized nanocrystalline 2 are about 245 nm in diameter, which exhibit much higher catalytic activities than those of large single crystal products of 2.

Experimental section

Materials and methods

All reagents for syntheses were commercially purchased and used without further purification. The ligand 1,4-bis-(1,2,4-triazol-1-ylmethyl) benzene (BBTZ) was prepared according to



Scheme 1 Schematic view of POM-based MOCNs in which POMs can act as (a) nodes, (b) templates, and (c) pillars (green balls represent POM units).

the reported procedure.¹⁴ $\text{H}_3\text{PW}_{12}\text{O}_{40} \cdot n\text{H}_2\text{O}$ and $\text{K}_5\text{BW}_{12}\text{O}_{40} \cdot n\text{H}_2\text{O}$ were prepared based on the literature methods.¹⁵ Elemental analyses (C, H and N) were conducted on a Perkin-Elmer 2400 CHN elemental analyzer. W, Co and Cu were determined by a Leaman inductively coupled plasma (ICP) spectrometer. The IR spectra were recorded in the range of 4000–400 cm^{-1} on an Alpha Centaur FT/IR spectrophotometer with pressed KBr pellets. The TG analyses were carried out under air flow by using a Pyris Diamond TG instrument at a heating rate of 10 °C min⁻¹. The powder X-ray diffraction (PXRD) patterns were collected by using a Rigaku D/max-IIb X-ray diffractometer with Cu-K α ($\lambda = 1.5418 \text{ \AA}$) radiation in the 2 θ range of 5° to 50° at a scanning rate of 1° per minute. The GC-MS spectra were obtained on an agilent 5875-6890N. The HPLC analyses were performed on a shimadzu LC-15C instrument.

Synthesis

[Co(BBTZ)_{1.5}(HBBTZ)(H₂O)₂][PW₁₂O₄₀]·H₂O (1). A mixture of $\text{H}_3\text{PW}_{12}\text{O}_{40} \cdot n\text{H}_2\text{O}$ (0.6g, 0.2mmol), $\text{Co}(\text{OAc})_2 \cdot 4\text{H}_2\text{O}$ (0.102 g, 0.4 mmol), and BBTZ (0.15 g, 0.625 mmol) was dissolved in 10 mL of distilled water at room temperature and stirred for 0.5 h. The pH of the reaction mixture was adjusted to about 4.0 with 1.0 M NaOH. The suspension was sealed in a 23 mL Teflon-lined autoclave and heated at 140 °C for 3 days. After slow cooling to room temperature, brown block crystals were filtered and washed with distilled water (65% yield based on W). Anal. calcd for $\text{C}_{30}\text{H}_{37}\text{N}_{15}\text{O}_{43}\text{PW}_{12}\text{Co}$: C 10.02, H 1.03, N 5.85, W 61.45, Co 1.65; found: C 10.22, H 1.09, N 5.64, W 61.39, Co 1.67. Selected IR (solid KBr pellet, cm^{-1}): 3421(m), 3129(w), 1634(m), 1522(s), 1436(m), 1378(w), 1280(s), 1221(w), 1124(m), 1078(s), 975(s), 898(s), 804(s). TG analysis suggests that the first weight loss in the temperature range of 50–200 °C corresponds to the loss of three lattice and/or coordinated water molecules.

[Co_{2.5}(BBTZ)₄(H₂O)₂][BW₁₂O₄₀]·4H₂O (2). A mixture of $\text{K}_5\text{BW}_{12}\text{O}_{40} \cdot n\text{H}_2\text{O}$ (0.4 g, 0.13 mmol), $\text{Co}(\text{OAc})_2 \cdot 4\text{H}_2\text{O}$ (0.102 g, 0.4 mmol), and BBTZ (0.15 g, 0.625 mmol) was dissolved in 10 mL of distilled water at room temperature and stirred for 0.5 h. The pH of the reaction mixture was adjusted to about 3.0 with 1.0 M HCl. The suspension was sealed in a 23 mL Teflon-lined autoclave and heated at 140 °C for 3 days. After slow cooling to room temperature, red-brown block crystals were filtered and washed with distilled water (78% yield based on W). Anal. calcd for $\text{C}_{48}\text{H}_{60}\text{N}_{24}\text{O}_{46}\text{BW}_{12}\text{Co}_{2.5}$: C 14.14, H 1.47, N 8.25, W 54.19, Co 3.62; found: C 14.16, H 1.40, N 8.21, W 54.21, Co 3.48. Selected IR (solid KBr pellet, cm^{-1}): 3413(s), 3124(w), 1617(m), 1527(s), 1426(m), 1352(w), 1278(s), 1216(w), 1135(s), 1017(m), 979(s), 924(s), 799(s). TG analysis suggests that the first weight loss in the temperature range of 50–210 °C corresponds to the loss of six lattice and/or coordinated water molecules.

[Cu(BBTZ)_{2.5}][BW₁₂O₄₀]₂·4H₂O (3). A mixture of $\text{K}_5\text{BW}_{12}\text{O}_{40} \cdot n\text{H}_2\text{O}$ (0.4 g, 0.13 mmol), $\text{Cu}(\text{OAc})_2 \cdot \text{H}_2\text{O}$ (0.105 g, 0.4 mmol), and BBTZ (0.15 g, 0.625 mmol) was dissolved in 10 mL of

distilled water at room temperature and stirred for 0.5 h. The pH of the reaction mixture was adjusted to about 5.0 with 1.0 M NaOH. The suspension was sealed in a 23 mL Teflon-lined autoclave and heated at 140 °C for 3 days. After slow cooling to room temperature, blue block crystals were filtered and washed with distilled water (55% yield based on W). Anal. calcd for C₁₂₀H₁₂₈N₆₀O₈₄B₂W₂₄Cu₅: C 16.93, H 1.51, N 9.87, W 51.91, Cu 3.74; found: C 16.96, H 1.53, N 9.82, W 51.95, Cu 3.78. Selected IR (solid KBr pellet, cm⁻¹): 3436(s), 3108(s), 1621(w), 1525(s), 1424(m), 1352(w), 1280(s), 1129(s), 999(w), 950(s), 902(s), 821(s). TG analysis suggests that the first weight loss in the temperature range of 45–220 °C corresponds to the loss of four lattice water molecules.

Preparation of nanocrystal of compound 2

The preparation of nanocrystalline compound 2 was similar to that of single crystal compound 2, except that the surfactant sodium doceetyl sulfate (SDS) (10 mg, 0.035 mmol) was added in the reaction system. The red-brown crystalline solid was filtered, washed with distilled water and ethanol alternately, and dried in an oven at 60 °C for 24 h (70% yield based on W). The nanocrystals with an average diameter of 245 nm were obtained based on the SEM images (Fig. 8). The nanocrystals were characterized by FT/IR spectroscopy (Fig. S20†), PXRD (Fig. 11 and S19†), and EDX (Fig. S23†).

The procedure for catalytic oxidative desulfurization

The catalytic oxidative desulfurization was performed with dibenzothiophene (DBT). In a typical case, the DBT (0.0735 g, 0.4 mmol) and the catalyst (0.075 mmol) were added to 5 mL of CH₂Cl₂ and stirred for 10 min. Then, TBHP (2 mmol) was added to the above mixture and heated at 50 °C for 3–7 h. An aliquot of the mixture was periodically removed and put into an ice chamber to stop the reaction. The identity of the product was ascertained by FT/IR and GC-MS, while the yield was obtained by HPLC analysis with a UV-vis detector at $\lambda = 254$ nm using an Inertsil SIL-100A C18 column. All analyses were performed with the mobile phase: CH₃CN:H₂O = 90:10 at an operating flow rate of 1 mL min⁻¹. After the reaction, the catalyst was recovered by centrifugation, washed with distilled water and anhydrous ethanol alternately, and then dried in an oven at 60 °C for 24 h.

The model oil was obtained by dissolving a desired amount of dibenzothiophene (DBT) in *n*-octane with a corresponding S-content of 500 ppm. Oxidation of dibenzothiophene in fuels was carried out by mixing 0.075 mmol of nanocrystalline compound 2 and 5 ml of model oil in a two-necked kettle equipped with a magnetic stirrer and a condenser. After that, a desired amount of TBHP was rapidly added into the above mixture under vigorous stirring at 50 °C. After the reaction, the residual sulfur content was removed by a polar extractant (for example, acetonitrile or 1-methyl-2-pyrrolidone), and monitored *via* HPLC analysis.

X-ray crystallography

Single-crystal X-ray diffraction data for compounds 1–3 were recorded by using a Bruker Smart Apex CCD diffractometer with Mo K α radiation ($\lambda = 0.71073$ Å) at a temperature of 298(2) K. All structures were solved by the direct method and refined by a full-matrix least-squares method on F^2 using the SHELXTL-97 crystallographic software package.¹⁶ All non-hydrogen atoms were refined anisotropically, except for the lattice water molecules. The hydrogen atoms on organic carbon atoms were fixed in calculated positions. Hydrogen atoms on water molecules cannot be assigned from the weak reflection peaks but were directly included into the final molecular formula. During the refinement of compound 3, a number of O atoms on the polyoxoanion are disordered in two positions with 50% occupancy for each. Furthermore, the restraint command “ISOR” was used to restrain non-H atoms with ADP and NDP problems in compounds 1–3. Moreover, the triazole and benzene rings of the BBTZ ligands in all three compounds were also restrained with the commands “AFIX 69”, “AFIX 59”, “DELU”, and “DFIX” so as to restrain the bond distance and angles of the organic ligands with chemically reasonable structural features. All above restrained refinements led to relatively high restraint values of 229, 270 and 1212 for compounds 1–3, respectively. In the final refinement, compound 2 exhibits solvent accessible voids but only three lattice water molecules can be clearly assigned from the residual peaks. Thus, the SQUEEZE program was further used to remove the contributions of disordered moieties from all of the observed structure factors.¹⁷ The new generated *hkl* file was further used to refine the final crystal data. Based on the elemental analysis, TG analysis and the SQUEEZE calculation result, another water molecule is directly included in the final molecular formula of compound 2. Crystal data and structural refinement for 1–3 are listed in Table 1. Selected bond lengths and angles of 1–3 are listed in Table S1–S3.† Crystallographic data for this paper has been deposited at the Cambridge Crystallographic Data Center: CCDC 1063971 for 1, 1063960 for 2, 1401904 for 3.

Results and discussion

Crystal structure of 1

Single-crystal X-ray diffraction analysis reveals that compound 1 crystallizes in the monoclinic space group *C*2/c, and the crystallographically asymmetric unit consists of one polyoxoanion [PW₁₂O₄₀]³⁻, one Co²⁺ (Co1) ion, one BBTZ bridging ligand, one monoprotonated HBBTZ ligand in general positions, another half BBTZ ligand lying about a two-fold axis, two coordinated water molecules connected to Co1 center, and one lattice water molecule (Fig. 1, 2 and S1†). The cationic metal-organic fragment [Co(BBTZ)_{1.5}(HBBTZ)(H₂O)₂]³⁺ contains one crystallographically independent Co²⁺ center which adopts a six-coordinated mode with four nitrogen atoms derived from four BBTZ ligands and two coordinated water molecules (Fig. S1†). The bond lengths of Co–N range from 2.087(2) to 2.232(2) Å and the N–Co–N bond angles vary

Table 1 Crystal data and structure refinement for 1–3

Compound	1	2	3
Formula	C ₃₀ H ₃₇ N ₁₅ O ₄₃ PW ₁₂ Co	C ₄₈ H ₆₀ N ₂₄ O ₄₆ BW ₁₂ Co _{2.5}	C ₁₂₀ H ₁₂₈ N ₆₀ O ₈₄ B ₂ W ₂₄ Cu ₅
M _r	3591.85	4073.53	8506.54
T/K	298(2)	298(2)	298(2)
Cryst. syst.	Monoclinic	Triclinic	Monoclinic
Space group	C ₂ /c	P ₁	C ₂ /c
a/Å	39.245(8)	11.7046(9)	51.260(4)
b/Å	15.242(3)	14.5353(11)	15.4783(10)
c/Å	23.514(5)	28.585(2)	24.3771(16)
α/°	90	85.5140(10)	90
β/°	115.77(3)	78.9940(10)	103.921(2)
γ/°	90	66.8170(10)	90
V/Å ³	12 666(4)	4388.3(6)	18 773(2)
Z	8	2	4
μ/mm	22.086	16.215	15.292
F(000)	12 768	3689	15 484
Refls	10 932	15 268	16 535
R _{int}	0.0868	0.0322	0.0560
GOF	1.022	1.026	1.024
R ₁ [I > 2σ(I)] ^a	0.0459	0.0420	0.0866
wR ₂ (all data) ^b	0.0986	0.1011	0.1822

^a R₁ = $\sum ||F_o| - |F_c|| / \sum |F_o|$. ^b wR₂ = $\sum [w(F_o^2 - F_c^2)^2] / \sum [w(F_o^2)^2]^{1/2}$.

from 91.0(7) to 169.0(6)°. The bond distances of Co–O are in the range of 2.095(1)–2.097(1) Å. It is worthy to note that the BBTZ ligands in this metal–organic cationic moiety can be divided into three groups which are labeled as L_a, L_b and L_c (Fig. 1a and S2†). The first group (L_a) adopts a *trans*-configuration and links adjacent two Co atoms into 1-D chains; the second group (L_b) possesses a *cis*-configuration and can be viewed as the “middle rail” that connects the adjacent 1-D chains to form a ladder-like chain; the third group (L_c) displays a *cis*-configuration and acts as the “dangling arm”, protruding on the upper and lower sides of the ladder. It is worthy to note that the third group (L_c) is mono-protonated and only one triazole group coordinates with the Co center. In the packing arrangement, the adjacent 1-D chains are hydrogen-bonded by the lattice water molecules (O3w), forming a porous 2-D supramolecular network on the bc plane (Fig. 2a and 2b and Fig. S3†). The guest Keggin-type

POM anions and lattice water molecules are encapsulated in these voids (Fig. 2). Furthermore, the adjacent POM-encapsulated 2-D supramolecular networks are parallel with each other on the bc plane, and stack into 3-D supramolecular frameworks (Fig. 2c and 2d).

Crystal structure of 2

Compound 2 crystallizes in the triclinic space group P₁ and the crystallographically asymmetric unit contains one Keggin-type polyoxoanion [BW₁₂O₄₀]^{5−}, two and a half Co²⁺ (Co1, Co2, Co3) ions connected to the polyoxoanion, four BBTZ bridging ligands, two coordinated water molecules and four lattice water molecules (Fig. 3, 4 and S4†). In 2, the Co3 atom lies on an inversion center, two BBTZ ligands lie in general positions while the other two lie about independent inversion centers. In 2, there are two types of metal–organic coordination polymer fragments, that is, the 1-D chain and the 2-D network (Fig. 3). The metal–organic 1-D chain possesses two crystallographically independent Co centers (Co1, Co2), which are hexa-coordinated with three N atoms derived from three BBTZ ligands, two O atoms derived from two polyoxoanions, and one coordinated water molecule (Fig. 3a, b and S4†). The bond distances of Co–N and Co–O are in the range of 2.094(6)–2.136(6) Å and 2.067(8)–2.173(9) Å, respectively. The bond angles of N(O)–Co–N(O) are in the range of 82.5(4)°–175.5(3)°. In the 1-D chain of compound 2, adjacent Co(1) ions are connected by the *cis*-BBTZ bridging ligands (L_a) to form a 1-D Co(1)–BBTZ chain (Fig. 3a). The adjacent Co(2) ions are linked by the *trans*-BBTZ ligands (L_b) to form a 1-D zigzag Co(2)–BBTZ chain (Fig. 3a). Meanwhile, other *trans*-BBTZ ligands (L_c) bridge two Co(1)–BBTZ chains and one zigzag Co(2)–BBTZ chain together to generate an unusual 1-D metal–organic chain with the “N”-type cross-section

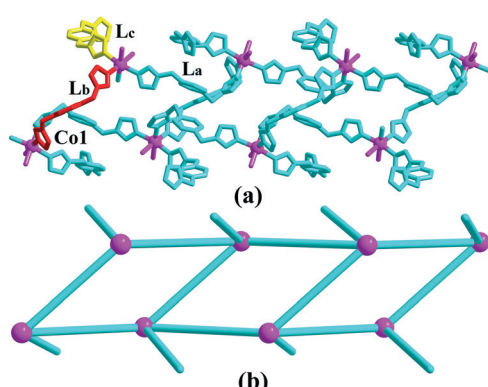


Fig. 1 (a) Ball-and-stick and (b) schematic views of the 1-D ladder-like chain unit in 1 formed by one Co²⁺ center and BBTZ ligands with three different kinds of structural configurations.

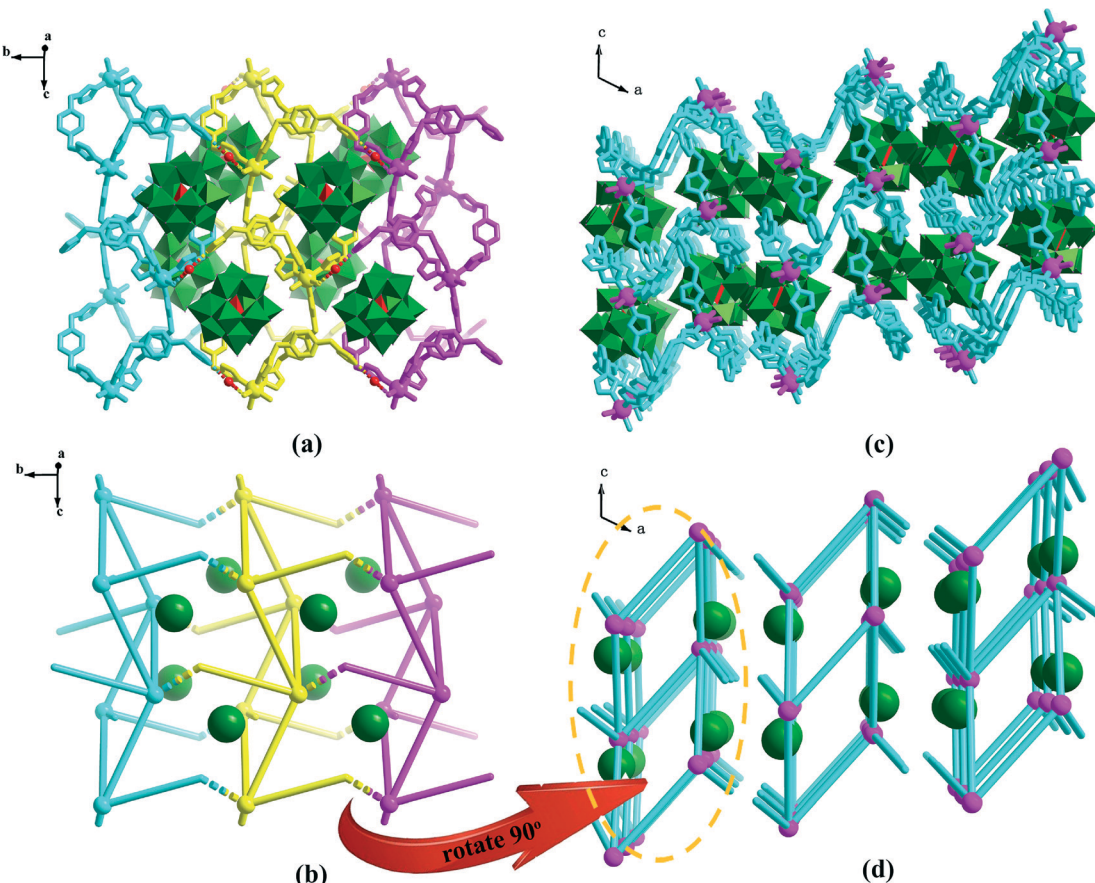


Fig. 2 (a) POM-encapsulated 2-D supramolecular network in **1** viewed along the *a* axis. 1-D ladder-like chains are shown in yellow, blue and purple for clarity. The lattice water molecules are shown as red balls. POM units are shown as green polyhedra. (b) Schematic view of the 2-D supramolecular network topology in **1** viewed along the *a* axis. (c) Polyhedral and ball-and-stick and (d) schematic views of the 3-D POM-encapsulated supramolecular network of **1** viewed along the *b* axis.

viewed along the *a* axis (Fig. S5†). The metal–organic 2-D network possesses one crystallographically independent Co center (Co3), which is hexa-coordinated with four N atoms derived from four BBTZ ligands and two O atoms derived from the two POM units (Fig. 4c and S4†). The bond lengths of Co(3)–N are in the range of 2.109(6)–2.117(6) Å and the

bond length of Co(3)–O is 2.148(8) Å. The bond angles of N(O)–Co–N(O) are in the range of 87.4(3)°–180°. In such 2-D network, all BBTZ ligands possess similar structural *trans*-configurations and link the Co(3) centers into a 2-D network with 4⁴ *sqp* topology (Fig. 3c and d). Each mesh is large with a size of 11.70(5) × 26.72(5) Å (Fig. S6†). In compound **2**, the cationic metal–organic 1-D chains and 2-D networks are connected by the Keggin-type polyoxoanions to form a POM-supported 3-D framework (Fig. 4 and S8†). From the topological viewpoint, the POM units can be viewed as a five-connected node, the Co(1) and Co(2) centers can be reduced to five-connected nodes, and Co(3) can be regarded as a six-connected node (Fig. S7†). Thus, the whole framework adopts the 4-nodal 5,5,5,6-*c* net with a stoichiometry of (5·c)₂(5·c)₂(5·c)₂(6·c), and the point symbol for the net is {3·4³·5²·6⁴}₂{3²·4·5⁴·6³}₂{4⁴·5⁴·6²}₂{4⁴·6¹⁰·8} (Fig. 4b).

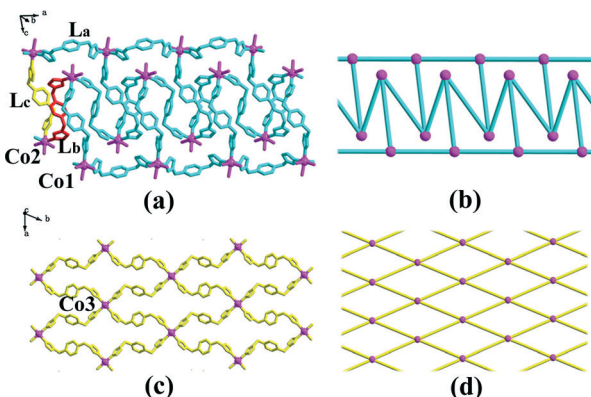


Fig. 3 (a) Ball-and-stick and (b) schematic views of the 1-D chainlike unit in **2**; (c) ball-and-stick and (d) schematic views of 2-D network moiety in **2**.

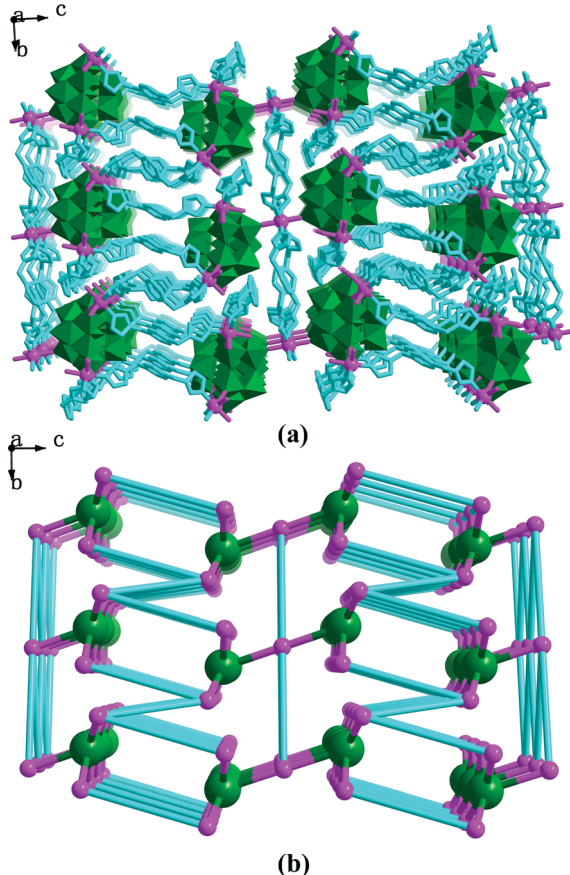


Fig. 4 (a) Polyhedral and ball-and-stick and (b) schematic views of the POM-supported 3-D network of **2** viewed along the *a* axis.

BBTZ bridging ligands and two lattice water molecules (Fig. S9†). It is also worth noting that the Cu2 center lies on a two-fold axis, three BBTZ ligands lie in general positions and two half BBTZ ligands lie about independent inversion centers. In **3**, three crystallographically independent Cu centers are all hexa-coordinated with four N atoms derived from four BBTZ ligands and two O atoms derived from two different POM units (Fig. 5, Fig. S9 and S10†). The bond lengths of Cu–N and Cu–O range from 2.004(1)–2.08(2) Å and 2.211(1)–2.791(1) Å, respectively. The five BBTZ ligands exhibit two types of structural configurations (Fig. S9†), that is, two *cis*-BBTZ ligands connect the Cu1 and Cu3 centers, while three trans-BBTZ ligands connect the Cu1–Cu3, Cu1–Cu2, Cu2–Cu2 and Cu3–Cu3 (generated by symmetry operations) centers, respectively. From the topological viewpoint, all three Cu centers can be reduced to a four-connection node. Thus, the whole cationic metal–organic framework adopts the 3-nodal 4,4,4-c net with a stoichiometry of $(5\text{-c})_2(6\text{-c})_2(6\text{-c})_2$, and the point symbol for the net is $\{3^2\cdot4^3\cdot5^4\cdot6^6\}_2\{3^2\cdot4^4\cdot5^4\}_2\{3^2\cdot4^5\cdot5^5\cdot6^2\cdot7\}_2\{4^2\cdot5^4\cdot6^8\cdot7\}$ (Fig. 6).

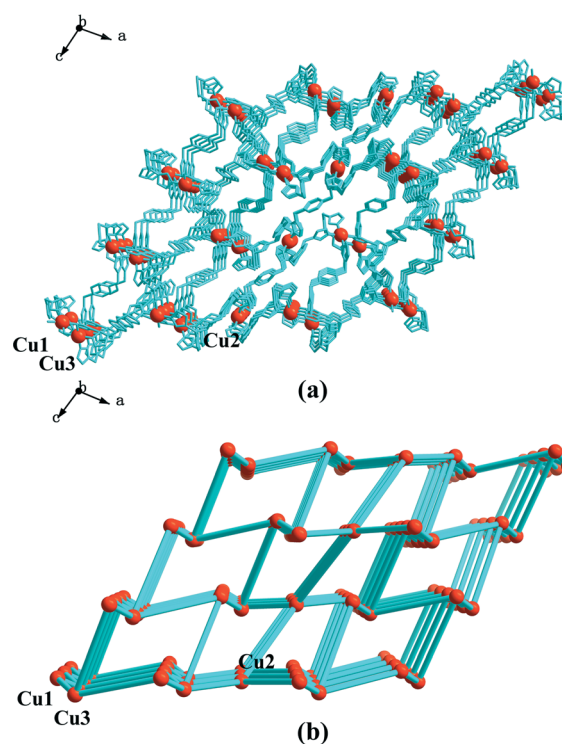


Fig. 5 (a) Ball-and-stick and (b) schematic views of the 3-D metal-organic network in **3**.

stoichiometry of $(5\text{-c})_2(6\text{-c})_2(6\text{-c})_2$, and the point symbol for the net is $\{6^3\cdot7^2\cdot8\}_2\{6^6\}_2\{7^4\cdot8^2\}$ (Fig. 5b). In such a cationic MOF framework, each guest Keggin-type POM unit also connects with five Cu centers *via* the Cu–O bonds, further stabilizing the whole framework. Thus, if the POM unit can be reduced to a five-connecting node, the whole framework shall adopt the 4-nodal 5,6,6,6-c net with a

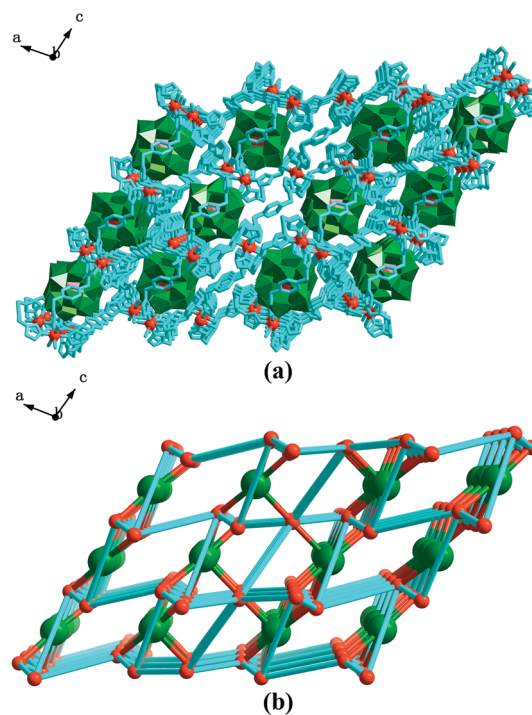
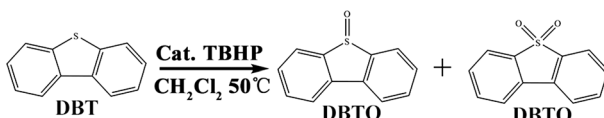


Fig. 6 (a) The chemical and (b) schematic views of the POM-supported 3-D open framework in **3**.



Scheme 2 Oxidation reaction of sulfide to corresponding sulfoxides and sulfones.

Catalytic oxidative desulfurization

The desulfurization of fossil fuels is one of the currently significant tasks, since their combustion waste can lead to serious atmospheric pollution, equipment corrosion and respiratory problems. In this research field, oxidative desulfurization has been developed as an effective approach to remove the refractory organosulfur compounds by the catalytic oxidation into corresponding sulfones under mild reactions.^{17–22} During the research process, dibenzothiophene (DBT) is usually employed as a typical refractory sulfur compound in fuels to evaluate the catalytic activities of test catalysts. In this case, the catalytic oxidation experiments of DBT with compounds 1–3 and a group of contrast catalysts were performed in a CH₂Cl₂ medium at 50 °C by using *tert*-butyl hydroperoxide (TBHP) as the oxidant (Scheme 2 and Table 2). The corresponding oxidized products were confirmed by FT/IR spectroscopy and GC-MS (Fig. S13 to S15†).

As shown in Fig. 7 and Table 2, compounds 1–3 all exhibit good catalytic activity on the oxidation of DBT into sulfoxide and sulfone. The maximum conversions can be observed after 7 h with the values of 91.57% for 1, 99.63% for 2 and 96.68% for 3, respectively, which are much higher than the conversion of 12.23% in the contrast group (without catalyst). As shown in Table S4,† compared with previous POM-based MOCNs catalysts, the catalytic activity of these three compounds has improved remarkably. In order to explore the catalytical active moieties of compounds 1–3, the catalytic activities of the precursors of compounds 1–3 were performed (see entry 5–12 in Table 2). It is found that the POM precursors exhibit obviously higher catalytic activity

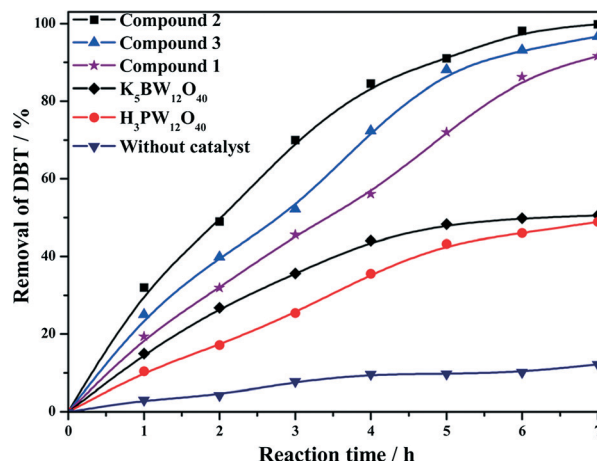


Fig. 7 Removal of the DBT versus reaction time with different catalysts.

than those of TM precursors (Fig. S16†). Thus, the POM units should be the catalytically active species in the composite coordination networks. This result is consistent with the reported catalytic mechanism of the POM species. The Mo/W centers of POMs may activate and/or “capture” the peroxy groups, forming peroxy-POM intermediates, which can oxidize sulfide into sulfoxide and/or sulfone. During the oxidative process, the peroxy-POM species are transferred into the POM species again and they enter into next catalytic cycle.^{19,20}

It is also worthy to note that the catalytic activities of compounds 1–3 are much higher than those of H₃PW₁₂O₄₀ and K₅BW₁₂O₄₀ POM salts (entry 5–6 in Table 2 and Fig. 7), indicating that the uniform dispersion of POM units into the metal–organic coordination networks in 1–3 at the molecular level may expose more POMs active sites, and thus remarkably improve the catalytic activities of the catalysts.

As shown in Fig. 7, the catalytic activity of K₅BW₁₂O₄₀ is slightly higher than that of H₃PW₁₂O₄₀. Therefore, the catalytic activities of compounds 1–3 are slightly different with the order of 2 (99.63%) > 3 (96.68%) > 1 (91.57%). These catalytic differences between compound 1 and 2–3 may be mainly derived from their difference in POM species. As a result of their crystal structures, the loading amount of POMs in MOCNs of 2–3 is 70.13% and 67.17%, respectively. So the tiny catalytic difference between compound 2 and 3 is probably due to the loading amount of the POM units, the different TM ions in the compounds (see entry 7–11 in Table 2) and the different network structural features of the two compounds. Especially, the last difference can be found from the powder X-ray diffraction patterns (PXRD). Generally, the strong diffraction peaks in the PXRD patterns exhibit the characteristic facets orientation of the crystalline compounds. In this case, the characteristic facets {002} of compound 2 expose more POM units than the characteristic facets {−111} of compound 3 (see Fig. S17†), suggesting that the characteristic facets containing more POM units may be an important factor that affects the activity of catalysts.

Another possible route to improve the catalytic property of these hybrid catalysts is to reduce the size of such crystalline

Table 2 Catalytic oxidation of sulfide to sulfoxide and sulfone with TBHP^a

Entry	Catalyst	Time/h	Conversion ^c (%)
1	Compound 1	7	91.57
2	Compound 2	7	99.63
3	Nanocrystal compound 2	3	99.74
4	Compound 3	7	96.68
5	H ₃ PW ₁₂ O ₄₀ ·nH ₂ O	7	48.94
6	K ₅ BW ₁₂ O ₄₀ ·nH ₂ O	7	50.61
7	Co(OAc) ₂ ·4H ₂ O	7	25.26
8	Cu(OAc) ₂ ·H ₂ O	7	23.03
9	K ₅ BW ₁₂ O ₄₀ ·nH ₂ O, Co(OAc) ₂ ·4H ₂ O ^b	7	65.39
10	K ₅ BW ₁₂ O ₄₀ ·nH ₂ O, Cu(OAc) ₂ ·H ₂ O ^b	7	62.82
11	H ₃ PW ₁₂ O ₄₀ ·nH ₂ O, Co(OAc) ₂ ·4H ₂ O ^b	7	63.79
12	None	7	12.23

^a Conditions: a mixture of catalyst (0.075 mmol), DBT (0.4 mmol), and TBHP (2.0 mmol, 5 equiv.) in CH₂Cl₂ (2 mL) was stirred at 50 °C.

^b Both POM and TM salt catalysts are 0.075 mmol. ^c The values are based on HPLC analysis.

catalysts, which can increase their specific surface area and expose more POM active sites during the catalytic process. In this case, the best efficient catalyst compound 2 is used as the representative sample to prepare the nanocrystallites. In this research field, the surfactant-assisted method has already been explored as an effective way to prepare nano-scale MOF materials, since the suitable surfactants can strongly influence the size of the crystals and control the nucleation rate for the production of highly crystalline materials.^{23–29} Up to date, the nanocrystallites of POM-based MOCNs prepared by this surfactant-assisted hydrothermal synthesis method have not been reported yet. During the preparation, the key factor is to choose suitable surfactants. Herein, we successfully prepared the nanocrystalline compound 2 by the use of anionic surfactant sodium dodecyl sulfate (SDS).^{30–33} The SEM images show that the uniform crystals have a rectangle morphology with a diameter of about 245 nm (Fig. 8). The powder X-ray diffraction (PXRD) pattern and EDAX of nanocrystal 2 are same as those of the large single-crystal 2, confirming the structural consistency (Fig. S19 and S23†).

The catalytic activity of nanocrystal 2 was studied under the same conditions. It is observed that the conversion of DBT can almost reach 100% after 3 h, indicating that the crystal size of the catalyst has an effect on the catalytic activity (Fig. 9) obviously. When the crystal size of catalyst 2 decreases, the specific surface area of the catalysts is dramatically improved, thus more POM active sites are exposed, leading to high catalytic activity. In such a catalytic reaction system, the nanocrystal 2 is insoluble and can be easily recycled by simple centrifugal separation (Fig. S18†). The recycling experiments reveal that the catalytic activity of the catalyst shows just a slight decrease after being reused for five cycles (Fig. 10), which might be related to the slight loss of catalyst

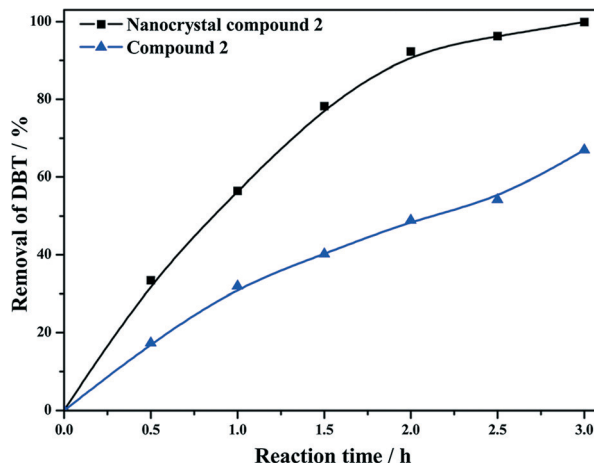


Fig. 9 Removal of DBT versus reaction time.

in the recycle process. The FT/IR spectra, UV-vis diffuse reflectance spectra and PXRD patterns (Fig. 11) of nanocrystal

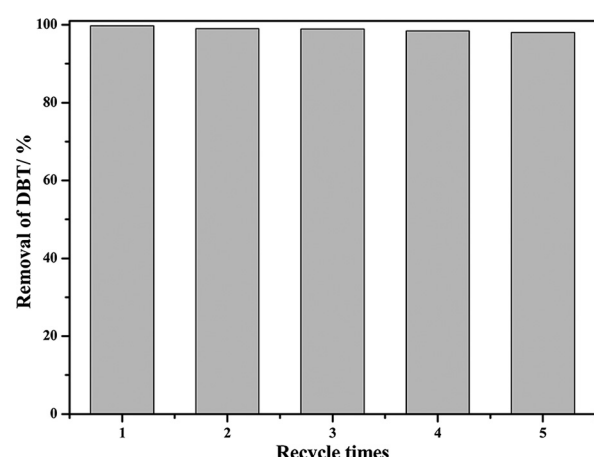


Fig. 10 The recycle experiments with nanocrystal 2 as catalyst.

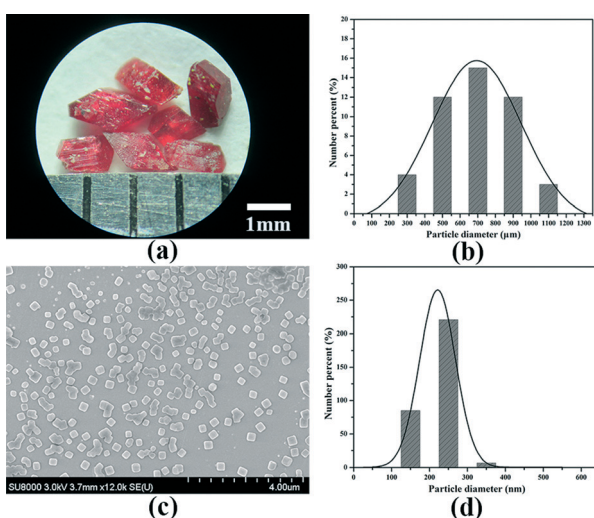


Fig. 8 (a) The images of the single crystals of 2 with the scale bar of 1 mm; (b) the particle size distribution of the single crystals of 2; (c) the SEM image of nanocrystals 2; (d) the particle size distribution of nanocrystals 2.

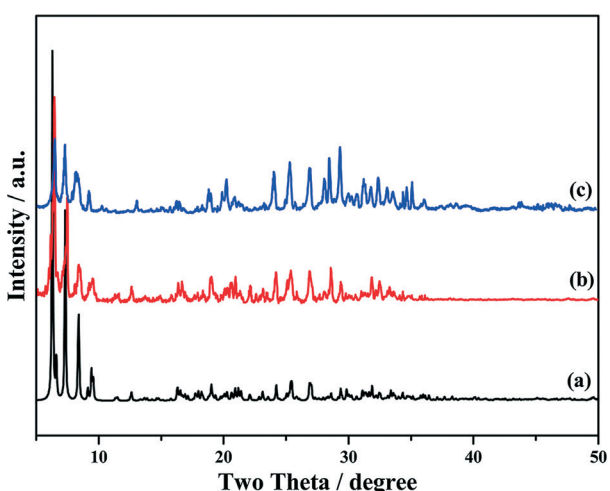


Fig. 11 PXRD patterns of nanocrystal 2 in the 2θ range of $5\text{--}50^\circ$ (a) simulated pattern; (b) as-synthesized sample of nanocrystal 2; (c) nanocrystal 2 after the catalytic reaction.

2 before and after five catalytic cycles (Fig. 11, S19–S21†) show a negligible change, suggesting that the nanocrystal 2 is stable in such a catalytic reaction system. In order to simulate the oxidative desulfurization in fossil oil, the catalytic activity of nanocrystal 2 in the model oil *n*-octane was also studied. The conversion of DBT can reach 100% after 3 h (Fig. S34†), manifesting that the nanocrystal 2 displayed excellent catalytic activity. The recycling experiments of nanocrystal 2 in *n*-octane also have been investigated and the conversion of DBT still reached 96.3% after 5 times of recycling without a significant decrease (Fig. S35†).

Conclusions

In summary, we presented three new Keggin-type POM-based metal–organic coordination networks. Compound 1 exhibits a POM-encapsulated 3-D supramolecular network, while compound 2 and 3 display the POM-supported 3-D coordination networks. All three compounds exhibited good catalytic activities in the heterogeneous catalytic oxidative desulfurization of DBT in contrast to their precursor POM salts, indicating that the monodispersion of POMs units in the metal–organic coordination networks at the molecular level can expose more active POM sites and increase the catalytic activity of the POM-based crystalline catalysts. In such non-porous POM-based MOCN catalysts, a series of factors such as the POMs species, transition metal cations, the loading amounts of POMs, and the structural features can affect their catalytic activities and the POM species are the main affecting factors. In order to further improve the catalytic activities of such type of catalysts, a new surfactant-assisted hydrothermal method for the preparation of nanocrystalline products has been developed. The uniform nanocrystals 2 were successfully prepared, which exhibit much better catalytic activity than the large single-crystal 2. This result confirms that reducing the size of crystalline catalysts can increase the specific surface area, expose more POM active sites, and thus improve the catalytic activity of the crystalline catalysts. This work confirms that the non-porous POM-based MOCNs can also be used as heterogeneous catalysts for the oxidative desulfurization and the preparation of uniform nanocrystalline POM-based MOCN products, and may pave new ways to explore such heterogeneous POM-based catalysts with high efficient catalytic activity. This work is still ongoing in our research team.

Acknowledgements

The authors gratefully acknowledge the financial support from the National Natural Science Foundation of China (grant no. 21271039, 21201032, 21471028 and 21401131), Program for New Century Excellent Talents in University (grant no. NCET120813) and Fundamental Research Funds for the Central Universities (grant no. 11SSXT140).

Notes and references

- (a) T. V. Choudhary, J. Malandra, J. Green, S. Parrott and B. Johnson, *Angew. Chem., Int. Ed.*, 2006, **45**, 3299; (b) A. Nisar, J. Zhuang and X. Wang, *Adv. Mater.*, 2011, **23**, 1130; (c) Z. Guo, B. Liu, Q. H. Zhang, W. P. Deng, Y. Wang and Y. H. Yang, *Chem. Soc. Rev.*, 2014, **43**, 3480; (d) O. Reimann, C. Smet-Noecca and C. P. R. Hackenberger, *Angew. Chem., Int. Ed.*, 2015, **54**, 306; (e) W. S. Zhu, C. Wang, H. P. Li, P. W. Wu, S. H. Xun, W. Jiang, Z. G. Chen, Z. Zhao and H. M. Li, *Green Chem.*, 2015, **17**, 2464; (f) W. W. He, G. S. Yang, Y. J. Tang, S. L. Li, S. R. Zhang, Z. M. Su and Y. Q. Lan, *Chem. – Eur. J.*, 2015, **21**, 1.
- (a) H. Y. Lü, J. B. Gao, Z. X. Jiang, Y. X. Yang, B. Song and C. Li, *Chem. Commun.*, 2007, 150; (b) S. Ribeiro, C. M. Granadeiro, P. Silva, F. A. A. Paz, F. F. D. Biani, L. Cunha-Silva and S. S. Balula, *Catal. Sci. Technol.*, 2013, **3**, 2404.
- (a) S. G. Mitchell, C. Streb, H. N. Miras, T. Boyd, D. L. Long and L. Cronin, *Nat. Chem.*, 2010, **2**, 308; (b) P. Putaj and F. Lefebvre, *Coord. Chem. Rev.*, 2011, **255**, 1642; (c) P. Huang, C. Qin, Z. M. Su, Y. Xing, X. L. Wang, K. Z. Shao, Y. Q. Lan and E. B. Wang, *J. Am. Chem. Soc.*, 2012, **134**, 14004; (d) X. B. Han, Z. M. Zhang, T. Zhang, Y. G. Li, W. B. Lin, W. S. You, Z. M. Su and E. B. Wang, *J. Am. Chem. Soc.*, 2014, **136**, 5359; (e) X. B. Han, Y. G. Li, Z. M. Zhang, H. Q. Tan, Y. Lu and E. B. Wang, *J. Am. Chem. Soc.*, 2015, **137**, 5486.
- (a) N. Mizuno, K. Yamaguchi and K. Kamata, *Coord. Chem. Rev.*, 2005, **249**, 1944; (b) D. Huang, Y. J. Wang, L. M. Yang and G. S. Luo, *Ind. Eng. Chem. Res.*, 2006, **45**, 1880; (c) D. Julião, A. Gomes, M. Pillnzer, L. Cunha-Silva, B. D. Castro, I. Gonçalves and S. S. Balula, *Fuel Process. Technol.*, 2015, **131**, 78; (d) J. X. Wu, W. Zhang, A. Tang, Y. L. Gao, Y. Y. Tan, Y. Men and B. H. J. Tang, *Inorg. Chim. Acta*, 2015, **425**, 108.
- (a) B. Keita, D. Bouaziz and L. Nadjo, *J. Electrochem. Soc.*, 1988, **135**, 87; (b) S. J. Dong, X. D. Xi and M. Tian, *J. Electroanal. Chem.*, 1995, **385**, 227.
- (a) F. Bigi, A. Corradini, C. Quarantelli and G. Sartori, *J. Catal.*, 2007, **250**, 222; (b) K. Yazu, Y. Yamamoto, T. Furuya, K. Miki and K. Ukegawa, *Energy Fuels*, 2001, **15**, 1535.
- (a) Y. Q. Lan, H. L. Jiang, S. L. Li and Q. Xu, *Adv. Mater.*, 2011, **23**, 5015; (b) C. Wang, K. E. dekrafft and W. B. Lin, *J. Am. Chem. Soc.*, 2012, **134**, 7211; (c) C. Y. Sun, X. L. Wang, X. Zhang, C. Qin, P. Li, Z. M. Su, D. X. Zhu, G. G. Shan, K. Z. Shao, H. Wu and J. Li, *Nat. Commun.*, 2013, **4**, 2717; (d) X. H. Liu, J. G. Ma, Z. Niu, G. M. Yang and P. Cheng, *Angew. Chem., Int. Ed.*, 2015, **54**, 988.
- (a) M. L. Wei, C. He, W. J. Hua, C. Y. Duan, S. H. Li and Q. J. Meng, *J. Am. Chem. Soc.*, 2006, **128**, 13318; (b) F. J. Ma, S. X. Liu, C. Y. Sun, D. D. Liang, G. J. Ren, F. Wei, Y. G. Chen and Z. M. Su, *J. Am. Chem. Soc.*, 2011, **133**, 4178; (c) H. Fu, C. Qin, Y. Lu, Z. M. Zhang, Y. G. Li, Z. M. Su, W. L. Li and E. B. Wang, *Angew. Chem., Int. Ed.*, 2012, **51**, 7985; (d) Z. M. Zhang, T. Zhang, C. Wang, Z. K. Lin, L. S. Long and W. B. Lin, *J. Am. Chem. Soc.*, 2015, **137**, 3197.
- (a) S. T. Zheng, J. Zhang and G. Y. Yang, *Angew. Chem., Int. Ed.*, 2008, **47**, 3909; (b) C. Y. Sun, S. X. Liu, D. D. Liang, K. Z.

- Shao, Y. H. Ren and Z. M. Su, *J. Am. Chem. Soc.*, 2009, **131**, 1883; (c) D. Y. Shi, C. He, B. Qi, C. Chen, J. Y. Niu and C. Y. Duan, *Chem. Sci.*, 2015, **6**, 1035.
- 10 R. Y. Hang, C. B. Du, S. J. Feng, C. L. Wang, Z. P. Kong, B. Yue and H. Y. He, *CrystEngComm*, 2011, **13**, 7143.
- 11 (a) S. X. Liu, L. H. Xie, B. Gao, C. D. Zhang, C. Y. Sun, D. H. Li and Z. M. Su, *Chem. Commun.*, 2005, 5023; (b) S. Yao, J. H. Yan, H. Duan, Z. M. Zhang, Y. G. Li, X. B. Han, J. Q. Shen, H. Fu and E. B. Wang, *Eur. J. Inorg. Chem.*, 2013, 4770; (c) S. B. Li, H. Y. Ma, H. J. Pang and L. Zhang, *Cryst. Growth Des.*, 2014, **14**, 4450.
- 12 (a) D. Y. Du, J. S. Qin, S. L. Li, Z. M. Su and Y. Q. Lan, *Chem. Soc. Rev.*, 2014, **43**, 4615; (b) W. W. He, S. L. Li, H. Y. Zang, G. S. Yang, S. R. Zhang, Z. M. Su and Y. Q. Lan, *Coord. Chem. Rev.*, 2014, **279**, 141.
- 13 (a) X. L. Hao, Y. Y. Ma, C. Zhang, Q. Wang, X. Cheng, Y. H. Wang, Y. G. Li and E. B. Wang, *CrystEngComm*, 2012, **14**, 6573; (b) X. L. Hao, Y. Y. Ma, Y. H. Wang, L. Y. Xu, F. C. Liu, M. M. Zhang and Y. G. Li, *Chem. - Asian J.*, 2014, **9**, 819; (c) X. L. Hao, Y. Y. Ma, W. Z. Zhou, H. Y. Zang, Y. H. Wang and Y. G. Li, *Chem. - Asian J.*, 2014, **9**, 3633; (d) X. L. Hao, Y. Y. Ma, H. Y. Zang, Y. H. Wang, Y. G. Li and E. B. Wang, *Chem. - Eur. J.*, 2015, **21**, 3778.
- 14 X. R. Meng, Y. L. Song, H. W. Hou, H. Y. Han, B. Xiao, Y. T. Fan and Y. Zhu, *Inorg. Chem.*, 2004, **43**, 3528.
- 15 R. D. Claude, F. Michel, F. Raymonde and T. Rene, *Inorg. Chem.*, 1983, **22**, 207.
- 16 (a) G. M. Sheldrick, *SHELXS-97, Program for solution of crystal structures*, University of Göttingen, Germany, 1997; (b) G. M. Sheldrick, *SHELXL-97, Program for refinement of crystal structures*, University of Göttingen, Germany, 1997; (c) A. L. Spek, *Acta Crystallogr., Sect. D: Biol. Crystallogr.*, 2009, **65**, 148–155.
- 17 Y. W. Liu, S. M. Liu, S. X. Liu, D. D. Liang, S. J. Li, Q. Tang, X. Q. Wang, J. Miao, Z. Shi and Z. P. Zheng, *ChemCatChem*, 2013, **5**, 3086.
- 18 N. Mizuno, K. Kamata and K. Yamaguchi, *Catal. Today*, 2012, **185**, 157.
- 19 (a) D. Liu, Y. Lu, H. Q. Tan, W. L. Chen, Z. M. Zhang, Y. G. Li and E. B. Wang, *Chem. Commun.*, 2013, **49**, 3673; (b) C. M. Granadeiro, A. D. S. Barbosa, S. Ribeiro, I. C. M. S. Santos, B. D. Castro, L. Cunha-Silva and S. S. Balula, *Catal. Sci. Technol.*, 2014, **4**, 1416; (c) M. Li, M. Zhang, A. M. Wei, W. S. Zhu, S. H. Xun, Y. N. Li, H. P. Li and H. M. Li, *J. Mol. Catal. A: Chem.*, 2015, **406**, 23; (d) S. H. Xun, W. S. Zhu, F. X. Zhu, Y. H. Chang, D. Zheng, Y. J. Qin, M. Zhang, W. Jiang and H. M. Li, *Chem. Eng. J.*, 2015, **280**, 256.
- 20 (a) W. S. Zhu, W. L. Huang, H. M. Li, M. Zhang, W. Jiang, G. Y. Chen and C. R. Han, *Fuel Process. Technol.*, 2011, **91**, 1842; (b) Z. X. Zhang, F. W. Zhang, Q. Q. Zhu, W. Zhao, B. C. Ma and Y. Ding, *J. Colloid Interface Sci.*, 2011, **360**, 189; (c) X. M. Yan, Z. K. Mei, P. Mei and Q. F. Yang, *J. Porous Mater.*, 2014, **21**, 729; (d) H. Y. Lü, C. L. Deng, W. Z. Ren and X. Yang, *Fuel Process. Technol.*, 2014, **119**, 87; (e) L. S. Nogueira, S. Ribeiro, C. M. Granadeiro, E. Pereira, G. Feio, L. Cunha-Silva and S. S. Balula, *Dalton Trans.*, 2014, **43**, 9518; (f) W. S. Zhu, B. L. Dai, P. W. Wu, Y. H. Chao, J. Xiong, S. H. Xun, H. P. Li and H. M. Li, *ACS Sustainable Chem. Eng.*, 2015, **3**, 186.
- 21 (a) W. S. Zhu, H. M. Li, X. Jiang, Y. S. Yan, J. D. Lu, L. N. He and J. X. Xia, *Green Chem.*, 2008, **10**, 641; (b) H. Y. Lü, Y. N. Zhang, Z. X. Jiang and C. Li, *Green Chem.*, 2010, **12**, 1954.
- 22 B. Y. Zhang, Z. X. Jiang, J. Li, Y. N. Zhang, F. Lin, Y. Liu and C. Li, *J. Catal.*, 2012, **287**, 5.
- 23 (a) L. H. Wee, S. R. Bajpe, N. Janssens, I. Hermans, K. Houthoofd, C. E. A. Kirschhock and J. A. Martens, *Chem. Commun.*, 2010, **46**, 8186; (b) L. H. Wee, N. Janssens, S. R. Bajpe, C. E. A. Kirschhock and J. A. Martens, *Catal. Today*, 2011, **171**, 275; (c) D. D. Liang, S. X. Liu, F. J. Ma, F. Wei and Y. G. Chen, *Adv. Synth. Catal.*, 2011, **353**, 733.
- 24 J. M. Yang, Q. Liu, Y. S. Kang and W. Y. Sun, *Dalton Trans.*, 2014, **43**, 16707.
- 25 R. Narayanan and M. A. El-Sayed, *J. Phys. Chem. B*, 2005, **109**, 12663.
- 26 M. J. Rosen and S. B. Sulthana, *J. Colloid Interface Sci.*, 2001, **239**, 528.
- 27 F. Zaera, *Chem. Soc. Rev.*, 2013, **42**, 2746.
- 28 M. Y. Ma, D. Zacher, X. N. Zhang, R. A. Fischer and N. Metzler-Nolte, *Cryst. Growth Des.*, 2011, **11**, 185.
- 29 Z. Ni and R. I. Masel, *J. Am. Chem. Soc.*, 2006, **128**, 12394.
- 30 A. Mirabi, A. S. Rad and H. Khodadad, *J. Magn. Magn. Mater.*, 2015, **389**, 130.
- 31 S. Hussain, T. M. Liu, N. Aslam, M. Kashif, S. X. Cao, M. Rashad, Y. Zhang, W. Zeng and M. S. Javed, *Mater. Lett.*, 2015, **152**, 260.
- 32 X. X. Xu, X. Gao, T. T. Lu, X. X. Liu and X. L. Wang, *J. Mater. Chem. A*, 2015, **3**, 198.
- 33 Y. J. Yang, A. V. Kelkar, X. L. Zhu, G. R. Bai, H. T. Ng, D. S. Corti and E. I. Franses, *J. Colloid Interface Sci.*, 2015, **450**, 434.